Contents lists available at ScienceDirect

Arabian Journal of Chemistry

journal homepage: www.ksu.edu.sa

Biomass-derived carbon/iron composite (FexOy-BC (RM)) with excellent Cd(II) adsorption from wastewater – Red mud resource utilization

Jiamin Qi [a,1], Hengxi Zhu [a,1], Tianyu Yang [a], Xingyuan Wang [a], Zixuan Wang [a], Xiaoli Lei [a], Bin Li [a,b,*], Wenmin Qian [c,*]

[a] Faculty of Environmental Science and Engineering, Kunming University of Science and Technology, Kunming 650500, Yunnan, China
[b] National-Regional Engineering Center for Recovery of Waste Gases from Metallurgical and Chemical Industries, Kunming 650500, Yunnan, China
[c] Yunnan Academy of Eco-Environmental Sciences, Kunming 650500, Yunnan, China

ARTICLE INFO

Keywords:
Red mud
Iron-carbon composite material
Cd(II)
Response surface
Renewability

ABSTRACT

Red mud is an industrial by-product produced in the process of alumina refining. It contains many iron elements, and the traditional resource utilization method is to extract it. This study took an alternative approach by using red mud's iron content as the substrate to synthesize a novel iron-biochar adsorbent for removing heavy metals from wastewater. Walnut shell biochar was reacted with the iron in red mud via an in-situ reduction–oxidation process to produce an iron-carbon composite adsorbent (FexOy-BC). A series of characterization analyses (e.g., SEM, FTIR, XPS, etc.) and batch adsorption experiments were conducted to investigate the properties and Cd(II) removal performance of the adsorbent, respectively. Response surface methodology was further employed to optimize the adsorption conditions, identifying the ideal 6 g/L adsorbent dose, 10 mg/L initial Cd(II) concentration (C_0), and pH 6. The optimized quadratic model demonstrated excellent fit, with an average Cd(II) removal efficiency of 92.59 % under optimal conditions. The adsorption mechanism, renewability, and preliminary cost-benefit analysis indicate that FexOy-BC has the potential to be a highly efficient and sustainable adsorbent. In summary, the new method can recover resources from red mud waste and synthesize heavy metal adsorbents, which comprehensively solves two long-standing problems of industrial waste.

1. Introduction

Red mud(RM) is a solid waste from the alumina production process, which can be classified into Bayesian RM, sintered RM, and combined RM according to the refining process. The compositions of RM produced by the three different methods are the same, while Bayerian RM is widely used in the research of iron recovery because of its high iron content (Wang et al., 2020). RM is characterized by solid alkalinity (pH = 9 ~ 12), rich in many kinds of heavy metals, fine particle size, high water content, etc., and if discharged randomly, it will cause serious harm to the environment (Hua et al., 2017). Currently, the treatment and disposal methods of RM are mainly open storage, which will not only occupy a large amount of land but also pollute the surrounding soil and groundwater and increase the ecological risk and pollution treatment costs (Yu et al., 2017). Currently, the total global RM stockpile has exceeded 4 billion tonnes and is growing at a rate of 200 million tonnes per year (Liu et al., 2021). From another perspective, RM is also a valuable resource, rich in iron and precious metal elements. If this part of the valuable resources can be recycled, it can turn RM into treasure.

Cd-containing wastewater has long been a global pollution problem, mainly from electroplating wastewater, smelting wastewater, printing and dyeing wastewater. Cadmium-containing wastewater, if discharged freely, will cause a severe threat to human health. Cd-containing wastewater into the soil has a muscular water mobility, and the surrounding environment is seriously harmful (Xie et al., 2018; Yang et al., 2020; Peng et al., 2021). Currently, the methods used to treat Cd-containing wastewater are mainly divided into three types: biological, chemical, and physicochemical processes and the physicochemical methods mainly include solvent extraction (Bilińska et al., 2019), adsorption (Truong et al., 2017; Chigondo et al., 2019), membrane

Peer review under responsibility of King Saud University. Production and hosting by Elsevier.
* Corresponding authors at: Faculty of Environmental Science and Engineering, Kunming University of Science and Technology, Kunming 650500, Yunnan, China (Bin Li).
E-mail addresses: 20212107029@stu.kust.edu.cn (J. Qi), libin@kust.edu.cn (B. Li), qwm_noon@yahoo.com.cn (W. Qian).
[1] These authors contributed equally to this work.

https://doi.org/10.1016/j.arabjc.2023.105411
Received 28 June 2023; Accepted 29 October 2023
Available online 31 October 2023

separation (Weng et al., 2013; Asuquo et al., 2017), and other physical forms, as well as advanced oxidation, ion exchange (Yan et al., 2019), chemical precipitation (Elzinga and Kretzschmar, 2013), photocatalysis, electrodialysis, electrodeposition, and electrochemical rainfall (Liu et al., 2018), chemical treatment methods such as electrochemical precipitation (Zhao et al., 2023), mixed polymerization, biological processes, etc., which take advantage of the physicochemical properties of chromium and the removal of Cd(II) is significantly affected by the surrounding environment (Fu and Huang, 2018). Biological methods are mainly based on the artificial cultivation of strains of bacteria that can adsorb Cd(II) to make reductants or flocculants. The advantages of the biological method are that it is effective in treating wastewater, can remove multiple heavy metal pollutants simultaneously, does not produce a large amount of residue, and is relatively less hazardous. However, the disadvantages of this method are slow removal rate, high cost of strain culture, and possible secondary pollution to the environment (Cai et al., 2021). The chemical method mainly utilizes the conversion of Cd(II) into $Cd(OH)_2$ for removal from water. It will produce a large amount of sludge, containing many Cd(II)-enriched substances, and cause secondary pollution. However, these methods are limited by technical and economic factors such as low selectivity, low efficiency, high association with health hazards, high energy consumption, and high amount of toxic substances used (Kong et al., 2022). Therefore, adsorption is one of the most influential and commonly used methods, which is currently an efficient and economical means of treating chromium-containing wastewater due to its high selectivity, ease of operation, environmental compatibility, high efficiency, energy saving, flexibility, simplicity, low cost, and wide availability, but some basic parameters must be controlled during the adsorption process (Kumar et al., 2018). Adsorbents that are widely recommended for the removal of heavy metals include industrial wastes, agricultural wastes, biological materials, and activated carbon. Carbon materials are the most commonly used adsorbents. Carbon adsorbents have high adsorption efficiency due to their loose, porous nature and large surface area. It includes biomass carbon and activated carbon, etc. The surface of activated carbon contains many active groups (−COOH, –OH, acid anhydrides, etc.), and more than 50 % of the activated carbon produced worldwide is currently used for water treatment. Among the various adsorbent materials, carbon materials are favored by researchers due to their diversity of raw materials and low cost and are considered to have the potential to remove heavy metals (Sikder et al., 2014).

Walnut shell(WS) belongs to agricultural and forestry waste, and its main components are lignin, cellulose, and hemicellulose (Calderon and Fullana, 2015). WS has excellent performance, which is a good carbon-based material for the treatment of wastewater because of its abundant raw materials, easy access to materials, low cost, and no secondary pollution (Calderon and Fullana, 2015). Although RM can pollute the environment, the excellent removal of heavy metals and other water pollutants by its properties has been proven. Whereas traditional carbon materials are expensive to synthesize and create environmental risk problems, iron-carbon composites are more accessible to prepare, environmentally friendly, and inexpensive. They are now becoming a research hotspot for treating heavy metal-containing wastewater.

In summary, in this study, bulk solid waste RM and agricultural and forestry waste WS were combined to prepare iron-carbon composites to remove pollutants from wastewater, which is an effective way to treat waste with waste and improve the utilization rate of solid waste resources. In this study, the high iron content of Bayer RM was used to selectively leach iron and exist as ferrous sulfate FeSO4-H_2O(RM), and FeOy-BC(RM), an iron-carbon composite material, was successfully prepared by in situ reduction and oxidation of ferrous sulfate $FeSO_4$-H_2O (RM) loaded on WS biocarbon, and FeOy-BC(RM), an iron-carbon composite, could be successfully prepared by in situ reduction and oxidation under the same conditions., FexOy-BC(RM) has higher adsorption efficiency under the same conditions. This study explores the adsorption conditions based on previous studies. It optimizes the experimental conditions for the adsorption of Cd(II) on FexOy-BC(RM) by combining with the response surface analysis method. Also, it explores the regeneration method and effect of FexOy-BC(RM) to reveal further the adsorption and regeneration mechanism of FexOy-BC(RM) and to provide ideas and techniques for the resourcefulness utilization of RM and WS. The novelty of this study lies in the fact that many of the current.

The novelty of this study lies in the fact that many researchers have focused on producing cheap natural adsorbent materials. At the same time, the agricultural and forestry waste walnut shells have a large specific surface area, more pore space, small fineness, and high adsorption activity, which can provide a carbon source for preparing porous composite materials. RM has a high iron content, and metal hydroxide flocs can remove heavy metals from water. Therefore, using this adsorbent not only solves the problem of WS and RM pollution but also reduces the preparation cost of adsorbent materials and reduces the waste of natural resources. Based on the resourceful use of solid waste, this study can also efficiently treat Cd-containing wastewater, achieving the treatment purpose of killing two birds with one stone.

2. Experimental part

2.1. Adsorbent material preparation

2.1.1. Iron extraction from red mud

The research used the Bayer red mud from an aluminum oxide plant in Wenshan, Yunnan province. The RM was dried to a constant weight at 60 ℃ in a standard oven. The RM was first washed with 3 M HCl (AR, Shanghai Maclin Biochemical Technology Co., LTD.) at T = 25 ℃, a solid–liquid ratio of 4:1 (Dry RM to 3 M solid–liquid ratio), and a speed of 600 rpm for 1 h. The solid–liquid mixture was filtered, and the acid-washed solution was collected and set aside. The RM was then pickled with $H_2C_2O_4$ (AR, Chengdu Colon Chemical Co., LTD.) and H_2SO_4 (AR, Shanghai Aladdin Biochemical Technology Co., LTD.) in a ratio of 3:3:2 (mass ratio) at T = 100 ℃, a solid–liquid balance of 16:1, and a speed of 600 rpm for 1.5 h. The solid–liquid mixture was filtered, and the pickling solution was collected and set aside (primary pickling solution). The RM from the direct acid leaching underwent secondary acid leaching under the same conditions as above to obtain the secondary acid leach solution, which was collected and set aside. Add 4 g of iron chips to the acid leach solution in a flask and stir it in a constant temperature water bath at T = 70 ℃ and 600 rpm for 1 h. The filtrate is collected after filtering the solid–liquid mixture for later use. Add 9 M H_2SO_4 to the filtrate and stir for 0.5 h in a constant temperature water bath at T = 60 ℃, with a 1:10 (solid–liquid ratio) and rotational speed of 600 rpm. Filter the solid–liquid mixture, collect the filtrate, and dry it under vacuum to constant weight. Grind the dried filtrate $FeSO_4{\cdot}H_2O$(RM) for 10 mins and set it aside for use.

2.1.2. Preparation of carbon/iron composite

WS was obtained from a market in Kunming, Yunnan Province, and dried in a constant temperature drying oven at 105 °C until it reached a stable weight. The dried WS was placed in the tube furnace (DHG-9240A, Shanghai Jinghong Laboratory Equipment Co., LTD.) under an N_2 atmosphere (N_2 flow rate = 60 mL/min) at 400 °C (heating rate = 5 K/min) for 3 h to produce the WS material precursor. The O_2-free ethanol aqueous solution was obtained using N_2 (N_2 flow rate = 60 mL/min) under anhydrous ethanol (AR, Chengdu Colon Chemical Co., LTD.): deionized water volume ratio = 3:1 and 600 rpm for 1 h after the O_2 was discharged.

Weighing 1.000 g of $FeSO_4{\cdot}H_2O$(RM) and dissolve it in 250 mL of the pre-prepared aqueous O_2-free ethanol solution to create a $FeSO_4{\cdot}H_2O$ (RM) solution. Weighing 0.500 g of $NaBH_4$ (AR, Shanghai Maclin Biochemical Technology Co., LTD.) and dissolve it in 250 mL of the previously prepared aqueous anaerobic ethanol solution to make a $NaBH_4$ solution. The $FeSO_4{\cdot}7H_2O$ solution was created by weighing

1.6360 g of $FeSO_4{\cdot}7H_2O$ and dissolving it in 250 mL of aqueous anaerobic ethanol. Under the same conditions, the material designed with $FeSO_4{\cdot}7H_2O$ was prepared as the FexOy-BC material.

The prepared $FeSO_4{\cdot}H_2O$(RM) solution and 0.3286 g of WS precursor were added to the 500 mL three-neck flask in a constant temperature water bath. The flask was first stirred with nitrogen gas for 3 mins, then 250 mL of $NaBH_4$ solution was added dropwise (dropwise acceleration rate = 10 mL/min) using a peristaltic pump for 30 mins and filtered. The filtrate was washed with an aqueous anaerobic ethanol solution 3–5 times and then dried in a vacuum oven at 70 °C to a constant weight to obtain FexOy-BC(RM). The material preparation process is shown in Fig. S1.

2.1.3. Experimental apparatus

The specific experimental process is as follows: Weighing a certain amount of adsorbent (RM, FexOy-BC(RM), FexOy-BC) and adding 25 mL of Cd(II) solution with a specific concentration. Adjusting the pH value with 0.5 M NaOH (AR, Shanghai Maclin Biochemical Technology Co., LTD.) or HCl, determining the pH value with a pH meter (DHS-3C, Shanghai, INESA Scientific Instrument Co., Ltd.), oscillating at 25 ℃, 140 r/min with a water bath constant temperature oscillator, and filtering the sample with 0.45um water filter after 8 h. The concentration of Cd(II) in the sample solution was measured by flame atomic absorption spectrometry (PHS-3C, Shanghai Yi Electrical Scientific Instruments Co., LTD). The effects of adsorbent addition amount, initial concentration of Cd(II), pH, and time on the adsorption efficiency of Cd (II) were investigated. Three parallel experiments were set up for all experiments in this study.

2.2. Analysis and calculation method

The hysteresis regression curve (VSM) was measured using MPMS-3 to determine the magnetic strength of FexOy-BC(RM). Scanning electron microscopy (SEM, ZEISS Sigma 300, Germany) was employed to examine the surface morphology of the samples before and after adsorption by the adsorbent. X-ray diffractometer (XRD, Rigaku Smartlab, Japan), the composition of samples were analyzed before and after adsorption under Cu Kα radiation. X-ray photoelectron spectroscopy (XPS, Thermo Scientific Nexsa, USA) was used to analyze the surface chemical composition of the samples before and after adsorption under monochromatic Al Kα X-ray source (1486.6 eV) conditions. Fourier transformed infrared spectroscopy (FTIR) spectrum of the FexOy-BC (RM) was obtained using a Nicolet IS10 spectrometer (Thermo Scientific iN10, America) at 4-cm^{-1} resolution. The C_0 in the solution and its concentration after the reaction were measured using atomic absorption spectrometry. The removal rate (Rt (%)) was calculated using **Equation (1)**, while the adsorption amount (Qt (mg/g)) was calculated using **Equation (2)**.

$$R_t(\%) = (C_0 - C_t)/C_0 \times 100\% \quad (1)$$

$$Q_t(\%) = V(C_0 - C_t)/m \quad (2)$$

Where:

R_t(%)—Cd(II) removal rate at equilibrium,%;
q_t—Cd(II) adsorption capacity at equilibrium, mg/g;
C_0—concentration of Cd(II) in solution before adsorption, mg/L;
C_t—Cd(II) concentration in solution after adsorption (concentration at equilibrium), mg/L;
V—solution volume (adsorbate volume), L;
m—the quality of adsorbent applied, g.

2.3. Response surface methodology (RSM)

Response Surface Methodology (RSM) is to Design the experimental method in the early stage rationally, then use the Design Expert software to analyze the experimental results and fit the relationship between influencing factors and variables. Finally, an intuitive 3D effect diagram and contour curve are obtained, and the values of factors affecting the optimal variables can be easily obtained from this result. The response surface method can consider the combination of elements in a broader range and predict the response value, which is more effective than the single-factor analysis method. The obtained relationship can determine the expected value at any test point within the test range, so it shows outstanding advantages.

Central Composite Design (CCD) and Box Behnken Design (BBD) are commonly used in the experimental design of the response surface method. The central composite design is suitable for creating 2 factors and above. Box Behnken design is mainly used to design three elements and more. To further analyze the adsorption test of Cd(II) in wastewater by FexOy-BC (RM) and find out the strength of the influence of various factors on the adsorption effect of Cd(II), the response surface method optimization test was carried out. This study uses Box Behnken to carry out the experimental design.

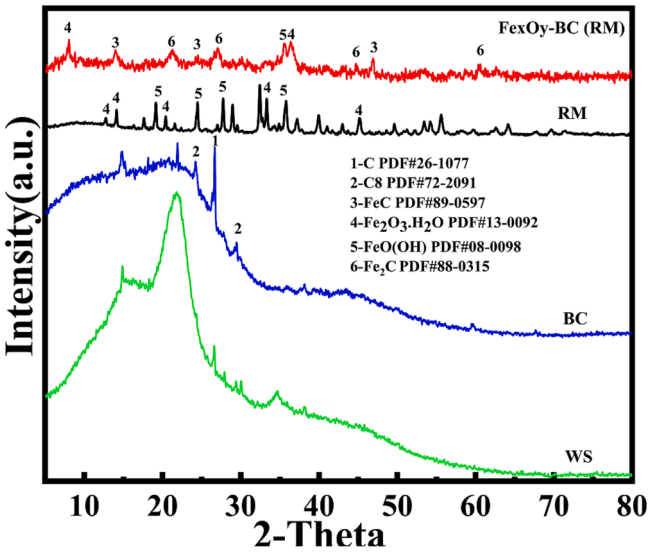

Fig. 1. XRD patterns of raw materials and FexOy-BC(RM).

3. Results and discussion

3.1. Characterization of FexOy-BC(RM)

3.1.1. XRF

The raw materials of RM and WS were initially tested for their XRF and organic element content. The results are shown in Tables S1-S3. It can be observed that RM is rich in Fe elements, providing a good source of Fe for preparing Fe-Carbon composites. WS has a high content of C element, indicating that it can supply carbon elements for composing FexOy-BC(RM). These characterizations demonstrate that RM and WS can provide a fundamental basis for preparing Fe-C composites.

3.1.2. XRD

XRD tests were conducted on the prepared FexOy-BC(RM) to analyze its physical phases in Fig. 1. When comparing the biochar and Fe-Carbon composites obtained after roasting WS, RM, and WS. It can be observed that the peaks in the FexOy-BC(RM) Fe-Carbon composites match well with RM, BC, and WS. New heights were also discovered in FexOy-BC (RM), located at 25.2° and 15.4°, primarily attributed to FeC、Fe_2C. Additionally, the characteristic peaks of Fe^0 are not present in the formed FexOy-BC(RM). These results indicate the formation of FexOy-BC(RM) and their complete oxidation.

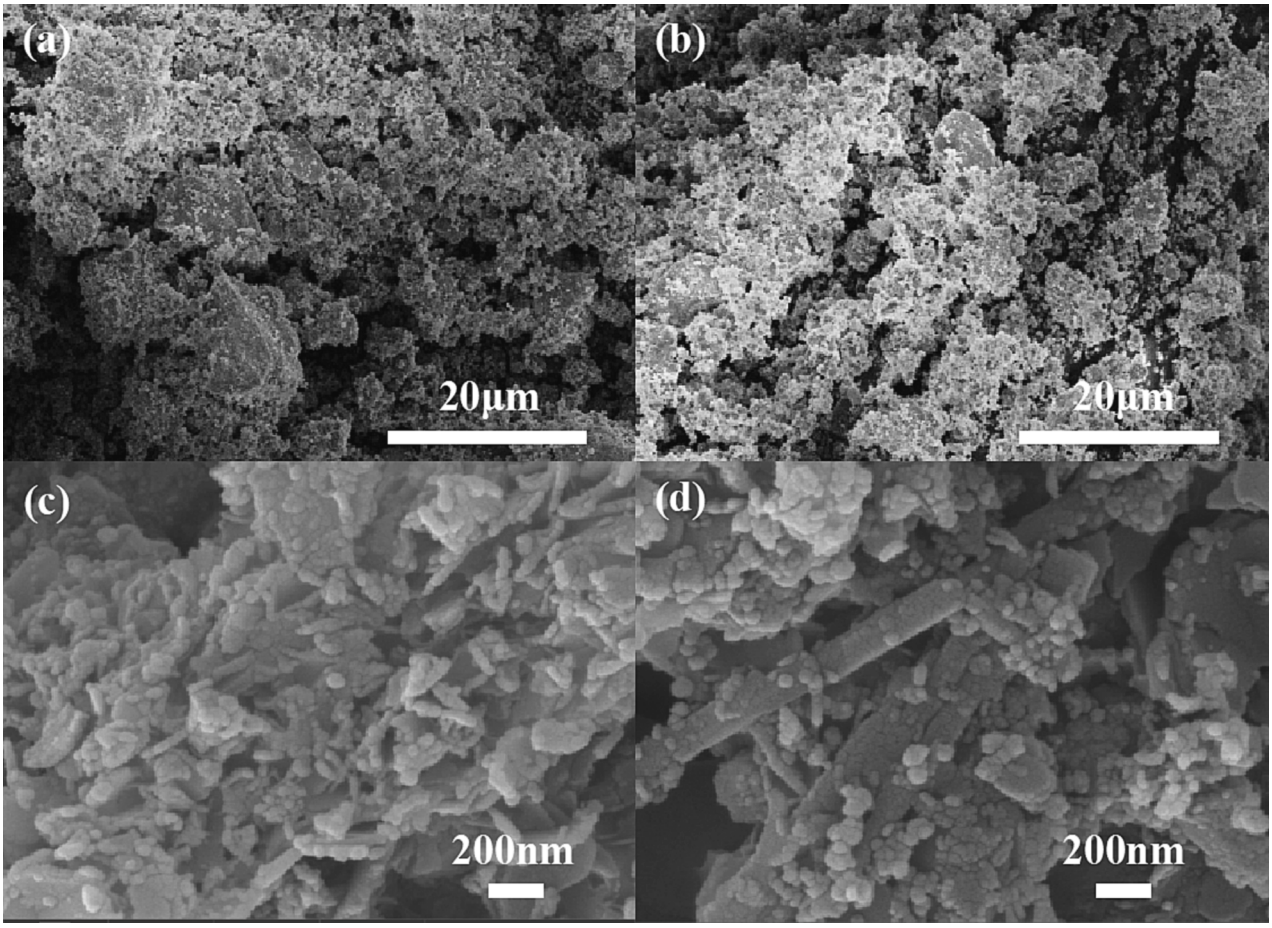

Fig. 2. SEM images of raw materials and FexOy-BC(RM): (a-b) natural red mud; (c-d) FexOy-BC(RM).

3.1.3. SEM

SEM characterization was conducted on RM, WS as is, and FexOy-BC (RM). The results are shown in Fig. 2. SEM characterization of the original RM sample and the synthesized FexOy-BC(RM) reveals that the original RM sample has an agglomerated structure. The synthesized FexOy-BC(RM) composites also possess the lamellar stacking structure of WS biochar. However, their particles are smaller and do not have agglomerated structures, providing more active sites for adsorption. In summary, the synthesized FexOy-BC(RM) has the structural basis of an adsorbent.

3.1.4. BET and particle size distribution

The structures of the raw RM and FexOy-BC(RM) were analyzed using a combination of BET and particle size distribution in **Table S4** and **Fig.S2**. and **Fig.S8.** The average particle size of FexOy-BC(RM) is 57.01 nm, which, based on BET and particle size distribution characterization results, is more extensive and provides more active sites for adsorption. The particles are well dispersed without accumulation, consistent with the results of SEM analysis. Compared to the raw RM, the FexOy-BC(RM) has an increased specific surface area, pore volume, and average pore size. The adsorption/desorption isotherm in Fig. S8**(a)** shows that the isotherm presents a type IV adsorption curve (Hua et al., 2017; Tang et al., 2020). When the relative pressure (P/P_0) is close to 0.80, the H3-type hysteresis loop of the double hydroxide structure material exists (Ain et al., 2020), and its shape is related to the porosity and shape of the porous material, indicating the existence of micropores and mesoporous pores in the adsorbent structure. The above results show that the adsorbents have the typical characteristics of mesoporous materials, and the pore structure is very irregular, including slit pores assembled by interconnected nanosheets (Huang et al., 2018). It can be seen from Fig. S8**(b)** that the pore size of the adsorbent is mainly distributed in the range of 2 ~ 60 nm, and the maximum pore size is 57.01 nm, which also proves that the adsorbent is especially mesoporous, and there are some medium/large pores (Li et al., 2016), indicating that the material has a multistage pore structure. Multistage pores are conducive to increasing the specific surface area of the material, providing adsorption sites, and improving the adsorption performance of the material (Ain et al., 2020).

These results indicate that doping WS can significantly increase the specific surface area and pore capacity of RM, improving its surface properties. It also shows that FexOy-BC(RM) has a structural basis as an adsorbent.

3.1.5. TEM

The prepared FexOy-BC(RM) was characterized using TEM in **Fig.S3**. It can be observed that the iron oxides are uniformly dispersed on the WS biochar, and the synthesized material has a core–shell structure. The lattice spacing $d_1 = 0.2646$ nm corresponds to the (−214) crystal plane of FeC, and $d_2 = 0.2660$ nm corresponds to the (101) crystal plane of $Fe_2O_3{\cdot}H_2O$, indicating that the FexOy-BC(RM) contain this material, consistent with the XRD analysis.

3.1.6. FTIR

As shown in **Fig.S9**, the characteristic peaks in the high-frequency region and the middle and low-frequency region mainly reflect the structure and component characteristics of FexOy-BC(RM). In the high-frequency part, 3460–3472 cm^{-1} is the stretching vibration peak of O–H or H_2O, and this peak occupies a larger area, indicating that the content of hydroxyl in FexOy-BC(RM) material is high, which plays a significant role in the precipitation of Cd (II) during the treatment process, proving

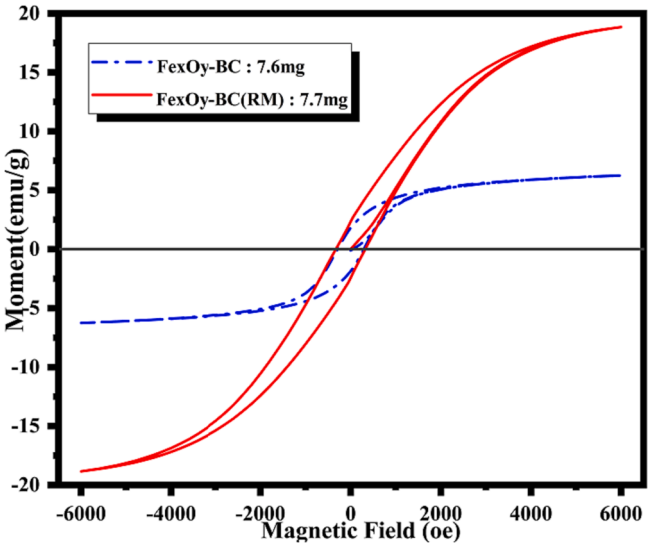

Fig. 3. Hysteresis regression curve (VSM) of iron-carbon composite materials.

that the adsorption is mainly chemisorption. It can also be seen that 1655 cm^{-1} corresponds to the disappearance of the peak after adsorption of C = O, indicating that C = O participates in the reaction, which is consistent with other characterization results. The peaks at 1406 and 1104 cm^{-1} correspond to –COOH, the mountains at 984 cm^{-1} are generated by -C = O, and those at 1385 cm^{-1} are caused by C-O tensile vibration mode(Chatterjee et al., 2009; Chowdhury et al., 2021). It can be seen that the –COOH position shifts after the reaction and is transformed into C-O or -C = O, indicating that –COOH is involved in the response. 628 and 692 cm^{-1} correspond to Fe-O, which proves that the adsorption is mainly chemisorption(Khan et al., 2007; Li et al., 2021).

3.1.7. Magnetic analysis of FexOy-BC(RM)

The hysteresis regression curve of the material was drawn to determine the magnetic properties of the iron-carbon composite. The result is shown in Fig. 3. The saturation magnetization of FexOy-BC(RM) is 18.845 emu·g^{-1}. Compared with FexOy-BC, it can be found that its saturation magnetization is stronger, indicating that the introduction of red mud can effectively enhance its magnetic properties and is more conducive to recovery from wastewater. The preliminary study shows that the magnetic properties of FexOy-BC(RM) may come from $Fe_2O_3{\cdot}H_2O$. The higher the muscle saturation magnetization of FexOy-BC(RM), the more obvious its advantage. The coercive force Hc and the remanent magnetization Mr(Li et al., 2021). Are almost near 0.

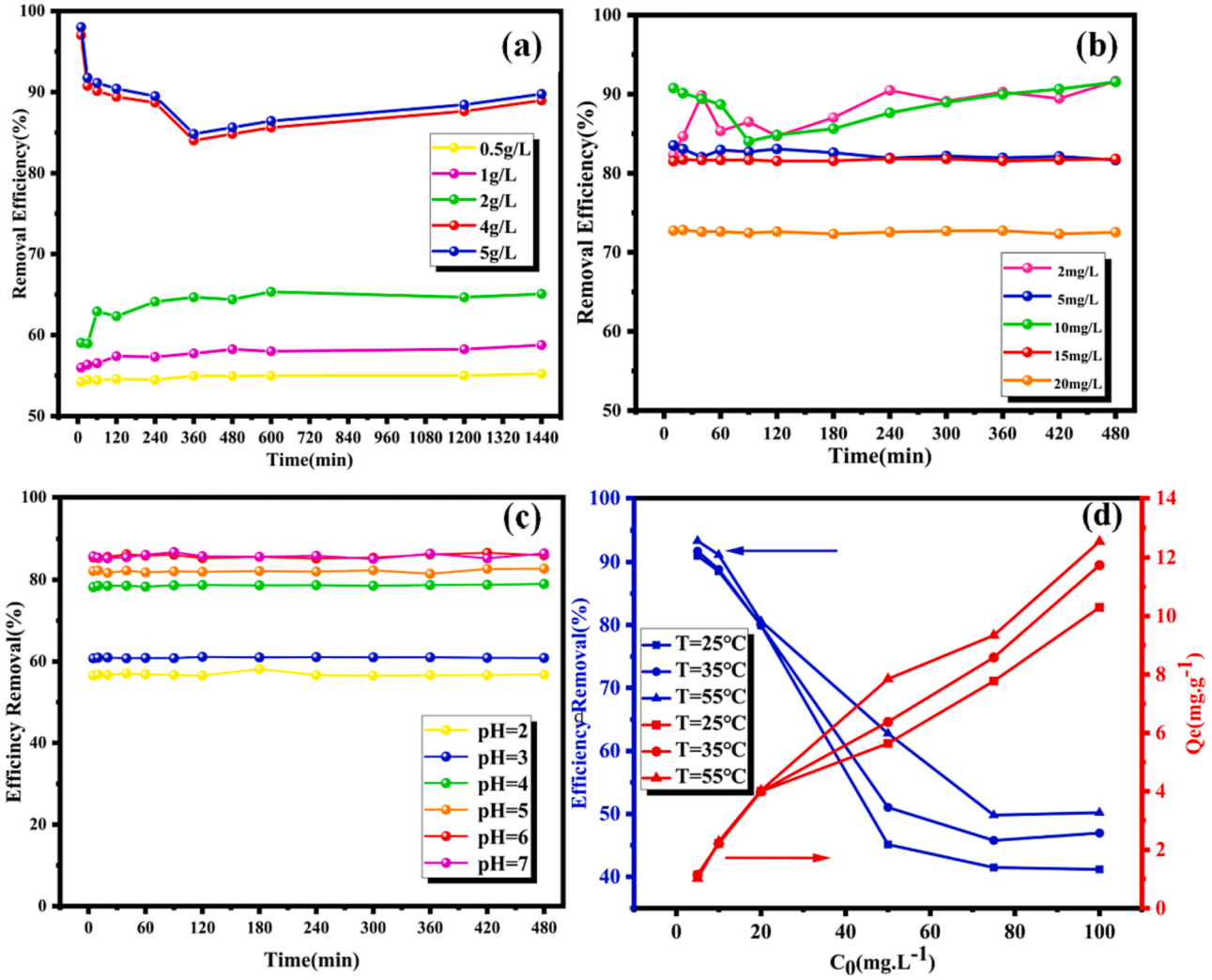

Fig. 4. Adsorption efficiency and capacity of FexOy-BC (RM) for heavy metal Cd(II) under different adsorption conditions (a) Adsorbent dosage; (b) Initial concentration C_0; (c) pH; (d) Temperature; (M = 4 g/L, t = 8 h, T = 25 ℃, C_0 = 10 mg/L, pH = 6).

However, its saturated magnetic susceptibility is much lower than the pure of FeO (148.9 emu·g^{-1}) because its composition is not magnetic. However, according to relevant literature studies, materials with a saturated magnetic susceptibility greater than 16.3 emu·g^{-1} are easily attracted by magnets, indicating that this adsorbent can be recovered by magnetic separation and recovery(Fu and Huang, 2018).

3.2. Optimization of adsorption parameters of FexOy-BC (RM) for Cd(II)

3.2.1. Effect of adsorbent dosage

Fig. 4**(a)** showed the change in adsorption efficiency when the adsorbent dosage added was 0.5 to 5 g/L, which was done to investigate the optimum amount of FexOy-BC(RM) adsorbent added for Cd(II). The adsorption efficiency also increased with an increase in adsorbent dosage from 0.5 to 5 g/L. The adsorption efficiency increased slowly when the adsorbent dosage = was 4 g/L. When the adsorbent dosage = 4 g/L, the adsorption efficiency was higher than 95.00 % in the first 5 mins and then decreased to 85.00 % before increasing again. According to the literature, this may be due to the re-release of Cd(II) adsorbed on FexOy-BC(RM). It may be due to incomplete oxidation of FexOy-BC(RM) in the oxidation process or a small amount of nZVI (Hu et al., 2005). Studies show that nZVI can adsorb Zn, Cd, Ni, Cu, and Cr. Except for Cr, all other metals have the phenomenon of re-releasing adsorbed pollutants. As nZVI is oxidized during adsorption, the pH value decreases, and nZVI surface crystallization occurs, reducing the adsorption efficiency. The adsorbent dosage is selected to be 4 g/L to ensure high adsorption efficiency and reduce adsorption cost.

3.2.2. Effect of initial concentration

As shown in Fig. 4**(b)**, the initial concentration (C_0) affects adsorption. The adsorption efficiency of FexOy-BC(RM) on Cd(II) gradually decreases with the increase in the C_0. Specifically, when C_0 = 2 mg/L, the adsorption efficiency can reach over 90.00 %. When the C_0 = 5 mg/L, the adsorption efficiency can be about 85.00 %. When the C_0 = 10 mg/L, the adsorption efficiency can reach over 85.00 %, which might be due to the increase in the driving force between Cd(II) and the adsorbent, increasing the utilization rate of active sites on the surface of the adsorbent. Therefore, the adsorption efficiency increased compared to when the C_0 = 5 mg/L. When the C_0 = 15 – 20 mg/L, the affinity of the active center for metal ions gradually decreases until the saturation point is reached. The total effective adsorption sites are limited to several adsorbents, so the adsorption efficiency gradually decreases (Hu et al., 2005). Therefore, the C_0 = 10 mg/L in follow-up experiments to achieve higher adsorption efficiency.

3.2.3. Effect of pH

As shown in Fig. 4**(c)**, pH affects adsorption efficiency. FexOy-BC (RM) quickly adsorbs Cd(II), and its adsorption efficiency increases with pH. The adsorption efficiency remains almost unchanged when the pH rises above 6, indicating that the optimal adsorption efficiency can be achieved when the pH = 6. When the pH = 4, the growth rate of adsorption efficiency increases. When the pH increased above 4, the growth rate of adsorption efficiency was slow. When the pH increased above 6, the adsorption efficiency was stable. Because as the pH value increases, the adsorption capacity will also increase. As the pH value increases, the negative charge on the adsorbent surface increases. Due to the deprotonation of –COOH and O–H, the negative charge on the adsorbent surface increases.

O–H leads to an increase in the negative surface charge of the adsorbent (Khan et al., 2020). Further expansion of pH = 7.0 did not increase the adsorption removal rate. However, when the pH value is more significant than 6.0, the removal rate slows down because when the pH value is more important than 6.0, the precipitation reaction predominates. It can be seen from other research that the adsorption of cadmium should be divided into two stages. The first stage is the simple adsorption of Cd^{2+} by the adsorbent, and the second stage of adsorption may be due to the fine precipitation of $Cd(OH)_2$ on the adsorbent at pH = 7.0. The adsorption behavior of Cd(II) is related to the pH value, which is caused by the protonation of the active site on the surface of the adsorbent. To achieve higher adsorption efficiency and save experimental resources, pH = 6 was selected.

Table 1
Response surface design factors and level.

Variable level	The adsorbent dosage (A) g. L^{-1}	The C_0 of Cd(II) (B) mg·L^{-1}	pH (C)
−1	2	5	2
0	4	10	4
1	6	15	6

3.2.4. Effect of temperature

Fig. 4**(d)** shows the effect of temperature on adsorption efficiency. In general, under the same C_0, the adsorption efficiency and amount of FexOy-BC (RM) for Cd(II) increase as the temperature increases from 25 - 55 ℃. Cd(II) adsorption by FexOy-BC (RM) is an endothermic reaction. Increasing the temperature promotes the dispersion and transfer of Cd (II) in the solution, promoting its adsorption on the surface of FexOy-BC (RM) and its removal (Yao et al., 2022). Additionally, the adsorption efficiency of Cd(II) on FexOy-BC (RM) decreased rapidly with the increase in C_0 from 5 - 100 mg/L, decreasing slowly until it reached 50 mg/L. The adsorption efficiency can reach above 80.00 %. Temperature does not affect adsorption efficiency. Therefore, from the perspective of saving resources, the temperature in this experiment is set at 25 ℃.

3.2.5. Contrast analysis

Adsorbent raw materials have a significant impact on the adsorption effect. To achieve higher adsorption capacity and efficiency, researchers mostly use chemical semi-finished products or chemical reagents combined with low-cost materials (agricultural and forestry waste, industrial waste residue) to prepare adsorbents, as shown in **Table S7**. However, few studies have used two kinds of garbage to prepare adsorbents. The adsorption pathways of Cd(II) by FexOy-BC(RM) in this study are as complex and diverse as those in other studies in the table and are highly efficient and feasible. In this study, FexOy-BC(RM), an iron-carbon composite material with excellent properties, was prepared from bauxite waste and agricultural and forestry waste WS, which not only reduced the preparation cost of adsorbent but also showed great potential for Cd(II) adsorption.

Table S8 shows that the adsorption capacity of this adsorbent for Cd (II) is higher than that of other studies. These differences may be due to the strong interaction between Cd(II) and the oxygen-containing functional groups on the surface of the adsorbent. Through the strong interaction of specific functional groups with them, a more substantial adsorption effect is generated, and the adsorption capacity is increased (Li et al., 2023).

3.3. Response surface optimization of Cd(II) adsorption by FexOy-BC (RM)

3.3.1. Factor and level design of response surface analysis

Several states that greatly influenced the adsorption efficiency were selected based on single-factor exploration to investigate the optimal adsorption conditions of Cd(II) by FexOy-BC (RM). Response surface analysis was established using the Box-Behnken (BBD) model in Design Expert 8.0.6 Trial. According to the kinetic study, the adsorption of Cd (II) by FexOy-BC (RM) can reach equilibrium in half an hour, so the time condition was not selected for optimization. Additionally, when the temperature rises from 25 - 55 ℃, the Cd(II) adsorption efficiency by FexOy-BC (RM) increases correspondingly. The effect of temperature on the adsorption efficiency was apparent. Three factors for response surface design were selected to reduce the experimental workload while

Table 2
Design and Results of Response Surface Experiment.

Run	The adsorbent dosage (A) g·L^{-1}	The C_0 of Cd(II) (B) mg·L^{-1}	pH (C)	Adsorption efficiency R_1,%
1	4	10	4	77.58
2	2	10	2	42.38
3	4	5	2	51.33
4	6	15	4	82.44
5	4	10	4	77.55
6	6	10	2	54.06
7	4	15	6	84.19
8	6	5	4	84.32
9	4	10	4	77.58
10	4	15	2	68.11
11	2	15	4	60.37
12	2	5	4	57.32
13	2	10	6	67.68
14	4	5	6	90.11
15	4	10	4	77.63
16	6	10	6	93.66
17	4	10	4	77.64

ensuring optimal experimental conditions: adsorbent dosage, C_0, and pH. Table 1 shows the factors and levels of response surface design. The adsorbent dosage (A) was 2, 4, and 6 g/L. The C_0 of Cd(II) (B) was 5, 10, and 15 mg/L. The pH was 2, 4, and 6. A response surface design with three factors and three levels was carried out. According to the three-factor response surface design, there were 17 experiments, the response surface design experiment and statistical adsorption efficiency in Table 2.

3.3.2. *Quadratic regression model fitting and variance analysis*

Multiple regression fitting analysis results can be obtained based on the design and response surface experiment results. The quadratic model is:

$$\text{Cd(II)adsorption efficiency}(\%) = 77.60 + 10.84A + 1.50B + 14.97C - 1.23AB + 3.57AC - 5.68BC - 7.74A^2 + 1.25B^2 - 5.41C^2 \quad (3)$$

Through the evaluation and statistical analysis of the model, the effects of the selected factors on the adsorption efficiency (%) (R_1) of heavy metal Cd(II) were determined. Table 3 shows the results of the variance analysis. An F-test can be used to measure the significance of each variable in the regression equation to the response value (adsorption efficiency). If $P_{(Prob)} > F$, the importance of the corresponding variable is higher ($P < 0.001$, hugely significant difference; $P < 0.01$, highly substantial difference; $P < 0.05$, significant difference; $P > 0.1$, no significant difference) (Li et al., 2023).

Table 3 shows the experimental results subjected to the variance analysis of the quadratic model of the response surface and effects. The salience of the model was changed to significant, with a significance level of $P < 0.0001$, indicating high effectiveness and statistical significance. The precision of the quadratic Equation was tested using *F*-test analysis of variance. The smaller the *P* value (Prob > *F*), the higher the significance of the corresponding variables ($P < 0.001$, extremely significant; $P < 0.01$, highly influential; $P < 0.05$, important; $P > 0.1$, not significant).

The results showed that the first-order variables A (the adsorbent dosage added) and C (the C_0) had a significant effect on the adsorption efficiency of Cd(II), with $P < 0.0001$. The simulated quadratic variables AC, BC, A^2, and C^2 were also significant, with $P < 0.05$. However, the simulated first-order variable B was insignificant, with $P > 0.1$. The *F* value directly reflects the influence of various factors on the response value; the more significant the *F* value, the greater the effect. Analysis of the impact of multiple factors showed that FC > FA > FB, indicating that the order of influence of various factors on Cd(II) adsorption efficiency was pH > adsorbent dosage > C_0.

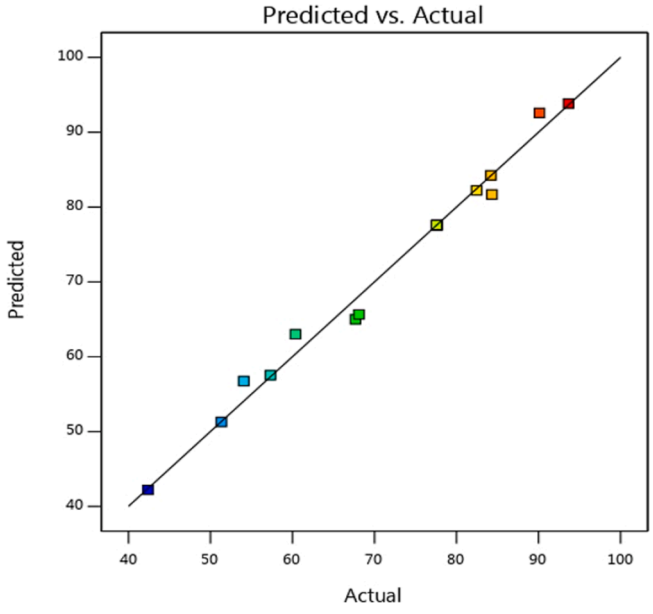

Fig. 5. Predicted and experimental adsorption efficiency.

Table 3
Results of variance analysis of quadratic regression equation.

Source	Sum of squares	d_f	Mean Square	*F*-Value	*P*-Value	Salience
Model	3333.46	9	370.38	63.83	<0.0001	significant
A- Adsorbent dosage	940.26	1	940.26	162.05	<0.0001	
B- C_0	18.09	1	18.09	3.12	0.1208	
C-pH	1792.81	1	1792.81	308.98	<0.0001	
AB	6.08	1	6.08	1.05	0.3402	
AC	51.12	1	51.12	8.81	0.0209	
BC	128.82	1	128.82	22.2	0.0022	
A^2	252.03	1	252.03	43.44	0.0003	
B^2	6.61	1	6.61	1.14	0.3211	
C^2	123.43	1	123.43	21.27	0.0024	
Residual	40.62	7	5.8	–	–	
Lack of Fit	40.61	3	13.54	9466.37	<0.0001	not significant
Pure Error	0.0057	4	0.0014	–	–	
Cor Total	3374.07	16	–	–	–	
C.V.%	3.35					
R^2	0.9880					
R^2adj	0.9725					
R^2pred	0.8074					

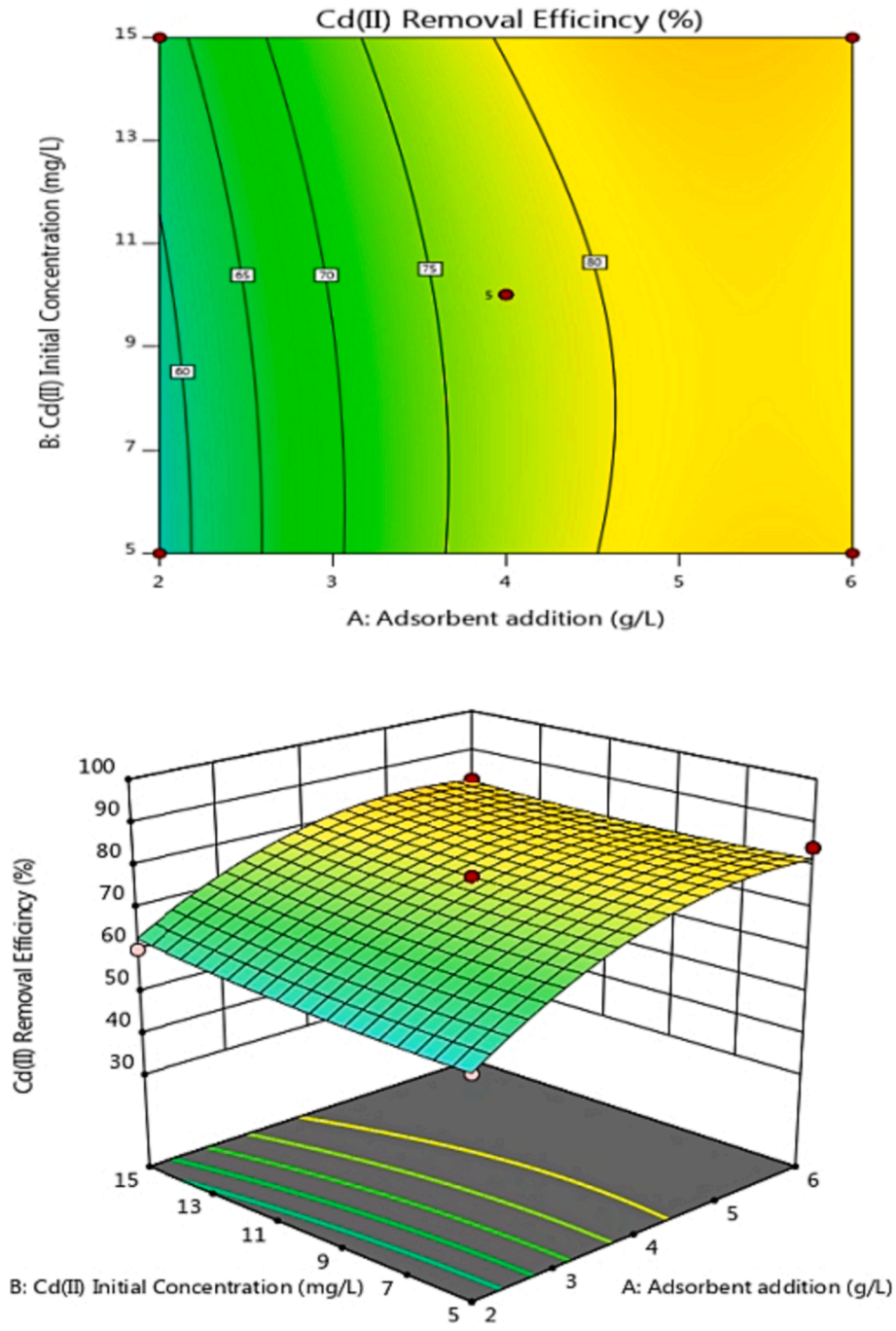

Fig. 6. Contour and response surface plot of the Effect of AB on adsorption efficiency.

As a function of the regression sum of squares (SSR) to the total sum of squares (TSS), the R^2 coefficient represents the proportion of variance predicted by the model. The model's R^2 value was 0.9880, indicating that it could explain 98.80 % of the experimental data. The adjusted R^2 value (R^2_{adj}) was 0.9725, indicating that the model could account for 97.25 % of the variation in response values. The difference between R^2_{adj} and the predicted R^2 value (R^2_{pred}) was 0.1651 (0.9725 - 0.8074), which is less than 0.2. The high and close values of R^2 and R^2_{adj} indicate that the model's test and prediction results are highly consistent and that the regression model can fully explain the test. The C.V% was 3.35 %, below 10 %, indicating a small experimental error and a good model fit (Weng et al., 2013; Gupta et al., 2011). In conclusion, the regression equation model provides a reasonably reliable preliminary prediction and analysis of heavy metal Cd(II) adsorption efficiency.

Fig. 5 compares the predicted and experimental Cd(II) adsorption efficiencies. This graph shows the linear correlation between experimental results and model predictions. Within the range of experimental error, the actual values are consistent with the expected values, indicating that the model is relatively reasonable.

3.3.3. *Contour maps and three-dimensional (3D) response surface analysis*

Adsorption efficiency was examined of Adsorbent dosage, C_0, and pH. Contour and 3D response surface graphs were plotted using Design-Expert software, as shown in Figs. 6–8. The color and slope changes in the maps reflect the effects of various factors on Cd(II) adsorption efficiency. On the contour map, the center of the smallest ellipse corresponds to the highest point on the response surface. When the contour is elliptical, the interaction between factors is more robust. The exchange

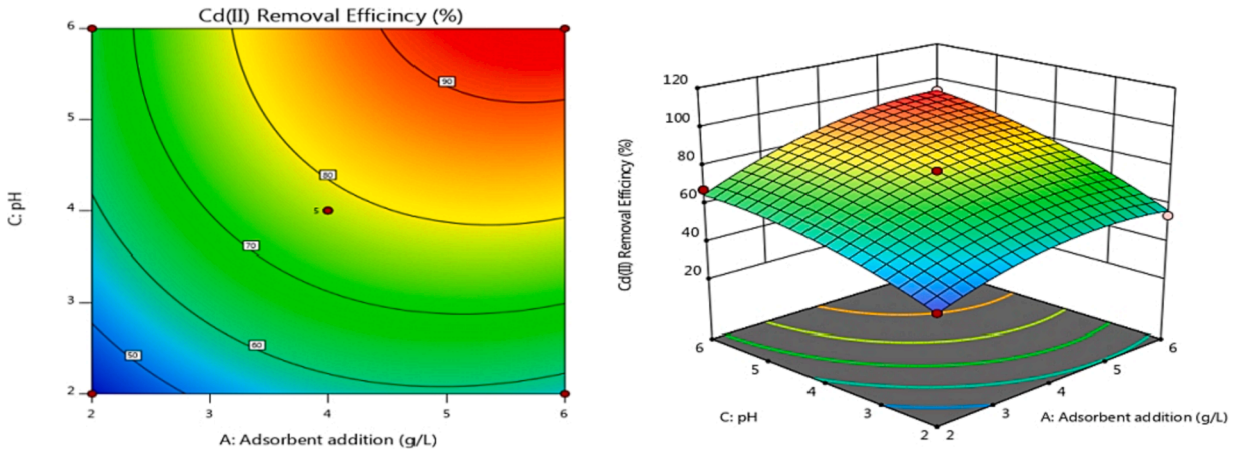

Fig. 7. Contour and response surface plot of AC effect on adsorption efficiency.

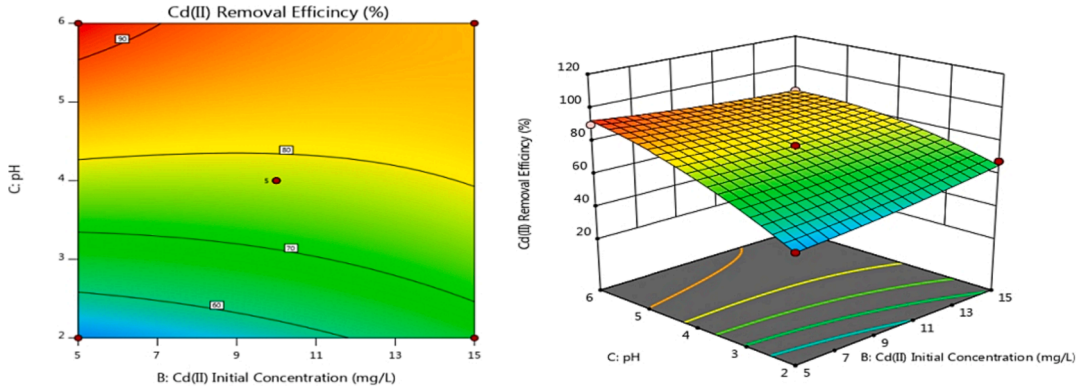

Fig. 8. Contour and response surface plot of BC effect on adsorption efficiency.

Table 4
Optimum experimental conditions determined by response surfaces.

Constraints	-	Lower	pper	Lower	Upper	-
Name	Goal	Limit	Limit	Weight	Limit	Importance
A	maximize	2	6	1	1	3
B	Is in range	5	15	1	1	3
C	Is in range	2	6	1	1	3
R_1	maximize	42.38	93.66	1	1	4
Solutions						
Number	A	B	C	R1		
12	6	10	6	93.831		
Parallel experiments		1	2	3	4	Average
Number		93.13 %	93.66 %	91.02 %	92.54 %	92.59 %

is not substantial if the contour lines are close to circular. The steeper the slope angle and the darker the color of the 3D response surface, the stronger the interaction and higher the adsorption efficiency for heavy metal Cd(II) (Lin et al., 2020). Fig. 6 shows that the AB contour line is nearly circular and that the slope angle of the 3D response surface is not very large, indicating that the interaction effect between the adsorbent addition amount and Cd(II) initial concentration is not very significant. The AC and BC contours are elliptical, indicating a substantial interaction between adsorbent addition amount and pH or Cd(II) initial concentration and pH, as shown in Figs. 7 and 8. These results are consistent with variance analysis of quadratic regression equations.

3.3.4. Determination and verification of optimum condition

According to the factor analysis in the Box-Behnken (BBD) model using Design Expert 8.0.6 Trial software, the optimum values of each reaction condition were predicted, and the optimum Cd(II) adsorption efficiency was estimated. The optimized experimental conditions were: an adsorbent dosage = 6 g/L, C_0 = 10 mg/L, pH = 6, and a predicted Cd (II) adsorption efficiency of 93.83 % in Table 4. Four parallel experiments were conducted to verify the optimal conditions in Table 4. Under the optimal conditions, the average Cd(II) adsorption efficiency was 92.59 %, close to the predicted value, indicating relatively accurate expected results.

3.4. Adsorption regeneration experiment

After using the adsorbent for the regeneration test, the optimized conditions were applied for adsorption experiments. The regeneration results are shown in Fig. 9, which indicates that the removal rate decreased slowly with increased cycles due to a small portion of the

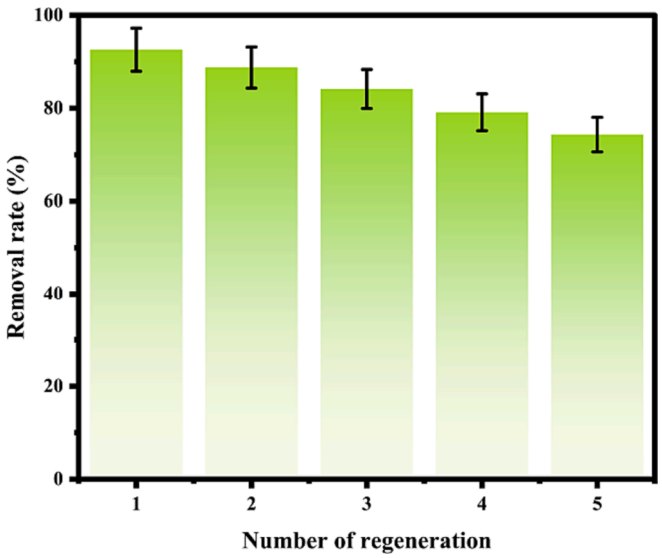

Fig. 9. Adsorption regeneration experiment.

adsorbent being lost with each process, reducing adsorbent mass and adsorption sites (Weng et al., 2013). The initial removal rate was 92.59 %, while the fifth removal rate stabilized at 74.33 %, showing good regeneration and stability of the material.

3.5. Reaction mechanism

The adsorption mechanism is shown in Fig. 10 and includes the following steps:

(1) The XPS diagram (Fig.S4) shows many oxygen-containing functional groups on the material surface, providing more active sites for Cd(II) adsorption. Comparing the C and O spectra of the oxygen-containing functional groups on the surface before and after adsorption, the content of C = C–C decreased while C-O-C and C-O increased, possibly due to oxidation. Comparing the Fe spectrum, the Fe-O-Fe content increases while the Fe-O range decreases, possibly due to C = C–C oxidation to C-O-C and Fe-O deterioration to produce more Fe-O-Fe.

(2) The adsorption kinetics results (Fig. S5 and Table S5) show that the maximum adsorption capacity calculated by the pseudo-second-order kinetics model is more consistent with the actual maximum adsorption capacity calculated, indicating that the pseudo-second-order kinetics has a better fitting effect. The results also suggest that the chemical interaction between heavy metals and the adsorbent mainly controls the adsorption rate of Cd(II) on the adsorbent. The pseudo-second-order kinetic adsorption mechanism depends on the concentration of adsorbent and adsorbent. Chemical adsorption is the primary method, and physical adsorption is the auxiliary method. The most crucial rate-limiting step is chemisorption. The sorbent sites available in this process play a vital role in the removal rate. The process that determines the adsorption process may involve the exchange of electrons between the adsorbent and the adsorbent, so the interaction force between the sharing and discussion of electrons during this adsorption process is also the main reason for limiting the reaction rate. The results show that the reaction is mainly based on chemisorption and accompanied by physical adsorption. The electron transfer in physical adsorption can effectively form Fe-O by trapping electrons through Fe^{2+}.

(3) Comparing SEM images before and after adsorption (Fig. S6), it can be seen that there are more pores on the material surface before adsorption, but they are blocked after adsorption, indicating physical adsorption.

(4) Combined with adsorption isotherm fitting and its parameters (Fig. S7 and Table S6), it can be found that adsorption conforms to the Freundlich model, which proves that multilayer adsorption is mainly based on chemical adsorption. According to the Freundlich model, *1/n* of the prepared adsorbent was between 0.1 and 0.5, indicating effective Cd(II) adsorption (Hua et al., 2017).

4. Conclusion

This study shows that many solid wastes RM can be used as iron-based composite materials with iron sources. Combined with other agricultural and forestry wastes, adsorption materials with excellent properties and simple and environmentally friendly preparation can be synthesized to absorb heavy metal Cd(II). Characterization tests were carried out for the adsorbent, showing that the prepared FexOy-BC (RM) has good superparamagnetism and can be quickly separated under an external magnetic field. The adsorbent dosage, C_0, pH, and T effects on adsorption efficiency were investigated. The optimal adsorption condition was: an adsorbent amount = 6 g/L, C_0 = 10 mg/L, and pH = 6. Response surface analysis (RSM) results show that the model analysis

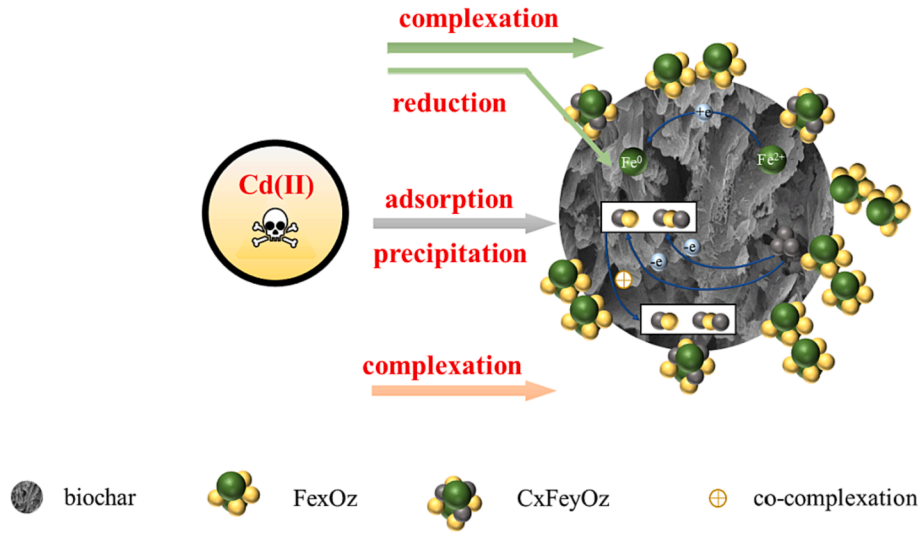

Fig. 10. Reaction mechanism.

results are reliable and consistent with experimental conditions. Under optimal conditions, the average adsorption efficiency of FexOy-BC (RM) on Cd(II) was 92.59 %. The Cd(II) removal rate remained 74.33 % after five adsorption cycles. Performance tests and characterization revealed the adsorption mechanism, indicating good reproducibility and stability of the material. It provides a new idea for treating industrial solid waste RM and heavy metal-containing wastewater.

Funding

This study was financially supported by the National Natural Science Foundation of China [52060010], Natural Science Foundation of Yunnan Province [202001AT07070088], the Low-carbon Development Guidance Project of Yunnan Province in the 2021 year (No.135).

CRediT authorship contribution statement

Jiamin Qi: Data curation, Formal analysis, Formal analysis, Writing – original draft. **Hengxi Zhu:** Investigation, Supervision, Writing – review & editing. **Tianyu Yang:** Methodology, Investigation. **Xingyuan Wang:** Methodology, Investigation. **Zixuan Wang:** Supervision, Resources. **Xiaoli Lei:** Methodology, Conceptualization. **Bin Li:** Supervision, Resources, Writing – review & editing. **Wenmin Qian:** Conceptualization, Data curation.

Declaration of Competing Interest

The authors declare that they have no known competing financial interests or personal relationships that could have appeared to influence the work reported in this paper.

Acknowledgements

The authors sincerely thank the anonymous reviewers, and this work was financially supported by the National Natural Science Foundation of China [52060010], Natural Science Foundation of Yunnan Province [202001AT07070088], the Low-carbon Development Guidance Project of Yunnan Province in the 2021 year (No.135).

Appendix A. Supplementary data

Supplementary data to this article can be found online at https://doi.org/10.1016/j.arabjc.2023.105411.

References

Ain, Q.U., Rasheed, U., Yaseen, M., Zhang, H., Tong, Z., 2020. Superior dye degradation and adsorption capability of polydopamine modified Fe3O4-pillared bentonite composite. J Hazard Mater 397, 122758. https://doi.org/10.1016/j.jhazmat.2020.122758.

Asuquo, E., Martin, A., Nzerem, P., Siperstein, F., Fan, X., 2017. Adsorption of Cd(II) and Pb(II) ions from aqueous solutions using mesoporous activated carbon adsorbent: Equilibrium, kinetics and characterisation studies. J. Environ. Chem. Eng. 5, 679–698. https://doi.org/10.1016/j.jece.2016.12.043.

Bilińska, L., Blus, K., Gmurek, M., Ledakowicz, S., 2019. Coupling of electrocoagulation and ozone treatment for textile wastewater reuse. Chem Eng J 358, 992–1001. https://doi.org/10.1016/j.cej.2018.10.093.

Cai, M., Zhang, Y., Dong, C., Wu, W., Wang, Q., Song, Z., Shi, Y., Wu, L., Jin, M., Dionysiou, D.D., Wei, Z., 2021. Manganese doped iron–carbon composite for synergistic persulfate activation: Reactivity, stability, and mechanism. J Hazard Mater 405, 124228. https://doi.org/10.1016/j.jhazmat.2020.124228.

Calderon, B., Fullana, A., 2015. Heavy metal release due to aging effect during zero valent iron nanoparticles remediation. Water Res 83, 1–9. https://doi.org/10.1016/j.watres.2015.06.004.

Chatterjee, S., Lee, M.W., Woo, S.H., 2009. Influence of impregnation of chitosan beads with cetyl trimethyl ammonium bromide on their structure and adsorption of congo red from aqueous solutions. Chem Eng J 155, 254–259. https://doi.org/10.1016/j.cej.2009.07.051.

Chigondo, M., Paumo, H.K., Bhaumik, M., Pillay, K., Maity, A., 2019. Magnetic arginine-functionalized polypyrrole with improved and selective chromium(VI) ions removal from water. J Mol Liq 275, 778–791. https://doi.org/10.1016/j.molliq.2018.11.032.

Chowdhury, A., Kumari, S., Khan, A.A., Hussain, S., 2021. Synthesis of mixed phase crystalline $CoNi_2S_4$ nanomaterial and selective mechanism for adsorption of Congo red from aqueous solution. J. Environ. Chem. Eng. 9, 106554 https://doi.org/10.1016/j.jece.2021.106554.

Elzinga, E.J., Kretzschmar, R., 2013. In situ ATR-FTIR spectroscopic analysis of the co-adsorption of orthophosphate and Cd(II) onto hematite. Geochim Cosmochim Acta 117, 53–64. https://doi.org/10.1016/j.gca.2013.04.003.

Fu, W., Huang, Z., 2018. Magnetic dithiocarbamate functionalized reduced graphene oxide for the removal of Cu(II), Cd(II), Pb(II), and Hg(II) ions from aqueous solution: Synthesis, adsorption, and regeneration. Chemosphere 209, 449–456. https://doi.org/10.1016/j.chemosphere.2018.06.087.

Gupta, V.K., Agarwal, S., Saleh, T.A., 2011. Chromium removal by combining the magnetic properties of iron oxide with adsorption properties of carbon nanotubes. Water Res 45, 2207–2212. https://doi.org/10.1016/j.watres.2011.01.012.

Hu, J., Chen, G., Lo, I.M.C., 2005. Removal and recovery of Cr(VI) from wastewater by maghemite nanoparticles. Water Res 39, 4528–4536. https://doi.org/10.1016/j.watres.2005.05.051.

Hua, Y., Heal, K.V., Friesl-Hanl, W., 2017. The use of red mud as an immobiliser for metal/metalloid-contaminated soil: A review. J Hazard Mater 325, 17–30. https://doi.org/10.1016/j.jhazmat.2016.11.073.

Huang, W., Chen, J., Zhang, J., 2018. Adsorption characteristics of methylene blue by biochar prepared using sheep, rabbit and pig manure. Environ Sci Pollut Res Int 25, 29256–29266. https://doi.org/10.1007/s11356-018-2906-1.

Khan, Z.H., Gao, M., Qiu, W., Islam, M.S., Song, Z., 2020. Mechanisms for cadmium adsorption by magnetic biochar composites in an aqueous solution. Chemosphere 246, 125701. https://doi.org/10.1016/j.chemosphere.2019.125701.

Khan, A.U.H., Iqbal, M., Islam, K.R., 2007. Dairy manure and tillage effects on soil fertility and corn yields. Bioresour Technol 98, 1972–1979. https://doi.org/10.1016/j.biortech.2006.07.041.

Kong, Y., Li, M., Zhou, Y., Pan, R., Han, Z., Ma, J., Chen, Z., Shen, J., 2022. Carbothermal synthesis of nano-iron-carbon composites for arsenate removal from high-arsenic acid wastewater. J. Environ. Chem. Eng. 10, 107140 https://doi.org/10.1016/j.jece.2022.107140.

Kumar, R., Kim, S., Kim, K., Lee, S., Park, H., Jeon, B., 2018. Removal of hazardous hexavalent chromium from aqueous phase using zirconium oxide-immobilized alginate beads. Appl Geochem 88, 113–121. https://doi.org/10.1016/j.apgeochem.2017.04.002.

Li, X., Liu, X., Huang, X., Lin, C., He, M., Ouyang, W., 2021. Activation of peroxymonosulfate by WTRs-based iron-carbon composites for atrazine removal: Performance evaluation, mechanism insight and byproduct analysis. Chem Eng J 421, 127811. https://doi.org/10.1016/j.cej.2020.127811.

Li, H., Qiu, R., Tang, Y., Duan, X., Gu, Y., Yang, H., Chen, Q., Shu, Z., Xiang, L., Liu, S., Tan, X., 2023. Formation of Fe(IV) over a wide pH range via iron-carbon composite-catalyzed persulfate activation. Chem Eng J 461, 141951. https://doi.org/10.1016/j.cej.2023.141951.

Li, B., Zhang, Y., Zhou, X., Liu, Z., Liu, Q., Li, X., 2016. Different dye removal mechanisms between monodispersed and uniform hexagonal thin plate-like MgAl–CO32–LDH and its calcined product in efficient removal of Congo red from water. J Alloys Compd 673, 265–271. https://doi.org/10.1016/j.jallcom.2016.02.248.

Lin, Y., Cong, R., Chen, Y., Fang, G., 2020. Thermal properties and characterization of palmitic acid/nano silicon dioxide/graphene nanoplatelet for thermal energy storage. Int J Energy Res 44, 5621–5633. https://doi.org/10.1002/er.5311.

Liu, X., Han, Y., He, F., Gao, P., Yuan, S., 2021. Characteristic, hazard and iron recovery technology of red mud - A critical review. J Hazard Mater 420, 126542. https://doi.org/10.1016/j.jhazmat.2021.126542.

Liu, J., Zhu, R., Liang, X., Ma, L., Lin, X., Zhu, J., He, H., Parker, S.C., Molinari, M., 2018. Synergistic adsorption of Cd(II) with sulfate/phosphate on ferrihydrite: An in situ ATR-FTIR/2D-COS study. Chem Geol 477, 12–21. https://doi.org/10.1016/j.chemgeo.2017.12.004.

Peng, Z., Lin, X., Zhang, Y., Hu, Z., Yang, X., Chen, C., Chen, H., Li, Y., Wang, J., 2021. Removal of cadmium from wastewater by magnetic zeolite synthesized from natural, low-grade molybdenum. Sci Total Environ 772, 145355. https://doi.org/10.1016/j.scitotenv.2021.145355.

Sikder, M.T., Mihara, Y., Islam, M.S., Saito, T., Tanaka, S., Kurasaki, M., 2014. Preparation and characterization of chitosan–caboxymethyl-β-cyclodextrin entrapped nanozero-valent iron composite for Cu (II) and Cr (IV) removal from wastewater. Chem Eng J 236, 378–387. https://doi.org/10.1016/j.cej.2013.09.093.

Tang, J., Zhang, Y., Liu, Y., Li, Y., Hu, H., 2020. Efficient ion-enhanced adsorption of congo red on polyacrolein from aqueous solution: Experiments, characterization and mechanism studies. Sep Purif Technol 252, 117445. https://doi.org/10.1016/j.seppur.2020.117445.

Truong, H.T., Nguyen, T.H., Lee, M.S., 2017. Separation of molybdenum(VI), rhenium (VII), tungsten(VI), and vanadium(V) by solvent extraction. Hydrometall. 171, 298–305. https://doi.org/10.1016/j.hydromet.2017.06.006.

Wang, H., Cai, J., Liao, Z., Jawad, A., Ifthikar, J., Chen, Z., Chen, Z., 2020. Black liquor as biomass feedstock to prepare zero-valent iron embedded biochar with red mud for Cr (VI) removal: Mechanisms insights and engineering practicality. Bioresour Technol 311, 123553. https://doi.org/10.1016/j.biortech.2020.123553.

Weng, X., Lin, S., Zhong, Y., Chen, Z., 2013. Chitosan stabilized bimetallic Fe/Ni nanoparticles used to remove mixed contaminants-amoxicillin and Cd (II) from aqueous solutions. Chem Eng J 229, 27–34. https://doi.org/10.1016/j.cej.2013.05.096.

Xie, W., Zhou, F., Bi, X., Chen, D., Li, J., Sun, S., Liu, J., Chen, X., 2018. Accelerated crystallization of magnetic 4A-zeolite synthesized from red mud for application in

removal of mixed heavy metal ions. J Hazard Mater 358, 441–449. https://doi.org/10.1016/j.jhazmat.2018.07.007.

Yan, S., Cai, Y., Li, H., Song, S., Xia, L., 2019. Enhancement of cadmium adsorption by EPS-montmorillonite composites. Environ Pollut 252, 1509–1518. https://doi.org/10.1016/j.envpol.2019.06.071.

Yang, T., Wang, Y., Sheng, L., He, C., Sun, W., He, Q., 2020. Enhancing Cd(II) sorption by red mud with heat treatment: Performance and mechanisms of sorption. J Environ Manage 255, 109866. https://doi.org/10.1016/j.jenvman.2019.109866.

Yao, Y., Pan, Y., Yu, Y., Yu, Z., Lai, L., Liu, F., Wei, L., Chen, Y., 2022. Bifunctional catalysts for heterogeneous electro-Fenton processes: a review. Environ Chem Lett 20, 3837–3859. https://doi.org/10.1007/s10311-022-01453-6.

Yu, Z., Dang, Q., Liu, C., Cha, D., Zhang, H., Zhu, W., Zhang, Q., Fan, B., 2017. Preparation and characterization of poly(maleic acid)-grafted cross-linked chitosan microspheres for Cd(II) adsorption. Carbohydr Polym 172, 28–39. https://doi.org/10.1016/j.carbpol.2017.05.039.

Zhao, Z., Li, Y., Zhou, Y., Hou, Y., Sun, Z., Wang, W., Gou, J., Cheng, X., 2023. Activation of sulfite by micron-scale iron-carbon composite for metronidazole degradation: Theoretical and experimental studies. J Hazard Mater 448, 130873. https://doi.org/10.1016/j.jhazmat.2023.13087.